08/05/94

Fermilab Library
0 1160 0039170 0

AUG 1 199

LYCEN-9429

LYCEN 9429
Juillet 1994

MICROSTRUCTURE OF NODULAR CAST IRON AFTER EXCIMER LASER SURFACE PROCESSING †

G. Marest[1)], A. Fontes[2)], J. Roigt[1)], A. Faussemagne[1)], S. Fayeulle[3)], M. Jeandin[2)], A. Benyagoub[1)], N.Moncoffre[1)], M. Frainais[4)].

1) *Institut de Physique Nucléaire de Lyon, IN2P3-CNRS et Université Claude Bernard, 43, Bd du 11 Novembre 1918, 69622 Villeurbanne Cedex, France.*
2) *Ecole des Mines de Paris, Centre des Matériaux P.M. Fourt, BP 87, 91003 Evry Cedex, France.*
3) *Ecole Centrale de Lyon, 36, Avenue Guy de Collongue, 69131 Ecully Cedex, France.*
4) *PSA-Peugeot Citroën, 9, Avenue du Maréchal Juin, 92366 Meudon La Forêt Cedex, France.*

ABSTRACT

Nodular iron of martensitic structure was treated by means of a XeCl laser prototype. The energy density varied from 0.3 J/cm^2 to 5 J/cm^2 and the number of shots from 4 to 40. Conversion electron Mössbauer spectroscopy, conversion X-ray Mössbauer spectroscopy and grazing incidence X-ray diffraction were used to characterize the irradiated surface. Some Rutherford backscattering spectrometry measurements were performed to control surface oxidation and carbon distribution.

It is shown that after irradiation austenite formed in a rather deep heat affected zone (10-20 μm) compared to the thickness of the melted zone ($\sim$ 1 μm). The austenite amount as well as its carbon content increase with energy density and number of shots up to a threshold of carbides formation. Beyond the threshold Fe_2C, Fe_3C and Fe_5C_2 formed only in the melted zone. The carbon content as a function of depth is constant in the melted layer then decreases quickly from the melted layer-heat affected zone interface down its initial value. Carbon content is shown to govern the evolution of phases content in the melted layer depending on the laser treatment conditions.

† *A paraître dans Hyperfine Interactions*

Introduction

Excimer laser is currently widely studied as a tool for processing metallic surfaces for a number of applications among which shallow remelting is of great interest. The process allows a shallow total heat affected zone (of about 1 to 10 micrometers in thickness) and controlled ablation due to short pulsed irradiation and good coupling of metals with ultraviolet (UV) radiation in contrast with that obtained when working in the infrared range typical of most industrial lasers. Excimer laser exposure may clean the surface of a metallic component [1] by ablating oxide, grease, dust and grinding inclusions while it may produce metallurgical transformations at the very surface by rapid melting and cooling [2] with out any change in the component dimension. The typical depth of the remelted layer is less than 5 micrometers depending on energy density above the melting threshold, surface roughness and thermo-physical properties of the processed material. For pure metals or alloys with no stable or metastable allotropic transformation near the base composition, no microstructural change occurs [3] and solidification consists of an epitaxial regrowth [4]. In contrast, if phase transformations occur it leads to refinement of the microstructure [5] (or amorphization for specific compositions [6]). In these cases the thin resolidified layer can enhance the material resistance against corrosion [7,8] or wear [9,10].

Cast iron is used in automotive industry for some friction engine parts (cylinder liner, camshaft, cranckshaft). Despite the creation of typical surface morphologies [11] leading to slight changes in roughness [12], excimer laser processing can improve dramatically the friction behavior of cast iron in severe conditions by decreasing the friction coefficient and the wear rate [9,10]. The wear rate of treated cast iron depends on laser treatment conditions due to modifications of several intricate superficial parameters (roughness, residual stress distribution, molten thickness layer, grain refinement and phase distribution) [9]. The influence of every superficial pa-

rameters on the friction behavior has to be isolated in order to elucidate mechanisms for improving the wear resistance. Prior to this, the microstructure of processed cast iron has to be investigated. The aim of the work presented in this paper is to characterize and discuss the formation of new phases in martensitic nodular iron treated using a XeCl laser (wavelength of 308 nm). The phases formed in both the resolidified zone and the heat-affected zone depending on laser energy density and number of laser pulses are studied.

One of the best techniques for characterizing the physico-chemical state of the affected layer is the Mössbauer spectroscopy. So far as CO_2 laser beams are used, classical transmission Mössbauer spectroscopy [13] and, more often, conversion X-ray detection were only used [14-18], the latter involving a layer of about 10 μm in thickness. For thin treated layers as those obtained by excimer laser treatment, detection of the conversion electrons after resonant absorption is more suitable since analysis is limited to a 0.1 - 0.2 μm thick layer. This was shown in recent studies for analysis of excimer laser-treated iron-based amorphous alloys [19] and steels [20].

Experimental

A nodular cast iron was processed using a XeCl laser prototype at the "Institut de Mécanique des Fluides de Marseille", Marseille, France. The wavelength of the laser beam is 308 nm and pulses of 50 ns full width half maximum time are generated at a repetition rate of 10 Hz or 30 Hz. The beam of energy up to 400 mJ was focused on a sample area of about 2 mm^2 yielding an incident energy density fluence in the 0.3 - 5 J/cm^2 range. The laser delivered up to 10 successive pulses per spot. For Mössbauer spectroscopy measurements the samples were $11 \times 10 \times 0.5$ mm^3 parallelepipeds, with the laser treatment onto the 11×10 mm^2 side area. Since the overlapping ratio was 50% along both directions of sample shifting, the number of

pulses has to be multiplied by 4 (up to 40 pulses locally) to obtain the actual number of pulses mentionned in the text. To measure the fluence, the energy of the beam was divided by the area of the melted surface. The chemical composition of the cast iron is reported in table 1. The initial fully martensitic microstructure of the samples was obtained by industrial induction heating in air. Before treating, the samples were prepared using conventional wet grinding followed by disc polishing using diamond paste down to 3 μm grit. The microstructure was revealed in cross-section by "Nital" etching (HNO_3 : 5 Vol % + Methanol : 95 Vol %).

The treated surfaces were observed by optical and Scanning Electron Microscopy (SEM), Conversion Electron Mössbauer Spectroscopy (CEMS), Conversion X-ray Mössbauer Spectroscopy (CXMS), Grazing Incidence X-ray Diffraction (GIXD) and Nuclear Backscattering Spectrometry (NBS). CEMS technique is a very powerful technique to probe the outermost layer of a material containing iron atoms. The probed thickness of about 150 nm has to be compared with the melted layer thickness of about 1 μm, so that only phases in the melted layer were detected. CEM spectra were determined at room temperature with the use of a flowing He-5% CH_4 gas proportional counter in which the sample was placed in a backscattering geometry. The ^{57}Co Rh source was mounted on a constant acceleration triangular motion velocity transducer. The velocity scale and all data are referred to metallic α-Fe absorber at room temperature. For spectra analysis two procedures were used. The first one consisted in a deconvolution of the spectra into sets of Lorentzian lines using a least squares fitting programme. The second was a programme developed by Le Caër *et al.* [21] in which hyperfine field distributions are considered. Some CXM spectra were recorded by changing He gas by Ar gas in the proportional counter. The CXMS technique allows to probe a depth layer of 10-20 μm. In order to follow the depth distribution of the phases produced in the melted layer electrochemical

etchings were performed using a bath containing perchloric acid (15 Vol %), acetic anhydre (80 Vol %) and water (5 Vol %). The depth of the etched layer was estimated with a good accuracy (better than 2%) from the weight loss by assuming that the polishing efficiency was identical for the irradiated and untreated surfaces.

NBS investigations were performed for analysing depth profiles of light (C, O,N) elements at the surface of treated cast iron. To have a good sensitivity for oxygen, nitrogen and carbon the energy of the α-particle beam was 7.5 MeV, 6.04 MeV and 5.7 MeV respectively. At these high energies we take advantage of the nuclear contributions in the cross section of the α, α' reactions.

Phases located into the melted zone were identified by GIXD measurements using a 2-circle vertical goniometer specially designed at the "Ecole Centrale de Lyon". Copper radiation was used without monochromator. A lithium doped silicon crystal was used as the detector and the Cu Kα radiation ($\lambda = 0.154$ nm) was selected owing to a multichannel analyser. The incident angle of the beam was varied between 0.3° and 3°, which allows to probe a depth layer from 40 nm to 0.4 μm.

Results

Figure 1a shows the typical superficial aspect of excimer laser-treated nodular iron. The nodules of graphite (average diameter 50 μm, 10 Volume%) did not melt but partially sublimated during laser-beam matter interaction. In contrast, the matrix is melted up to 3 μm depth depending on the laser conditions. Figure 1b shows a well marked melted zone of 2 μm in depth for a sample irradiated with 40 laser pulses of 5 J/cm^2 at 1 Hz. Other observations on treated samples show typical depths of melted zone of 1 μm.

Figures 2, 3 and 4 show examples of CEMS spectra obtained with a nodular iron irradiated with 1 J/cm^2, 1.5 J/cm^2 and 3 J/cm^2 beam energy densities and with dif-

ferent numbers of pulses. Before laser treatment, the CEMS spectrum is complex and was fitted by means of five magnetically split subspectra which hyperfine magnetic fields are equal to 33.7 T, 32.9 T, 28.0 T, 30.8 T, 18.8 T and a central paramagnetic doublet in addition. This last component has for hyperfine parameters : isomer shift IS = 0.4 mm/s, quadrupole splitting QS = 0.90 mm/s. It could be attributed to some surface oxidation of the sample or to very small superparamagnetic carbides [22]. The three first magnetic components are characteristic of a martensitic matrix [23,24], the component with B=30.8 T is due to the presence of alloying elements whereas the lowest field should be due to carbides formed by aggregation of C in α' matrix. After irradiation these carbides are dissolved even for the lowest fluence (0.5 J/cm^2) and the amount of the component with B = 30.8 T decreases strongly as much as the number of pulses is high.The main modification produced by the laser treatment in the CEMS spectra is the presence of a non-magnetic component in the central part of the spectra of all treated samples. Even after irradiation with one pulse of 0.3 J/cm^2 (near the melting threshold according to CEMS observations), this component was found. In fact, the central part is an overlapping of the preexistent quadrupole doublet with lines due to austenite. This austenite was fitted with three different iron environments as proposed by Bauer *et al.* [25] : two single lines $\Gamma_{0,0}$ (IS = $-0.10(1)$ mm/s) and $\Gamma_{0,n}$ (IS = 0.10(2) mm/s) and a quadrupole doublet $\Gamma_{1,0}$ (IS = 0.02 mm/s, QS = 0.63(3) mm/s) where in $\Gamma_{i,j}$, i and j are the number of C atoms in the first and second nearest neighbour shells respectively. For a given fluence, the amount of austenite increases with the number of shots. For example, in table 2, are summarized the relative contributions of the different phases present in CEMS spectra taken after irradiation at 2 J/cm^2 for 4, 8, 20 and 40 shots respectively. The comparison of figures 3 and 4 clearly shows that for a given number of pulses, the relative quantity of austenite increases with the fluence (fig. 5). However,

when the fluence is rather high (3 J/cm^2) and for a number of pulses higher than 20 shots a broad distribution of hyperfine fields is produced (fig. 6a) at the expense of austenite as the amount of martensite decreases continously with the fluence. After substracting the components due to the matrix and to the paramagnetic components it remains a spectrum which looks like a Mössbauer spectrum of amorphous material (fig. 6b). This spectrum was fitted using the Le Caër and Dubois programme [21] by assuming a hyperfine field distribution (HFD) in which hyperfine parameters are IS = 0.19 mm/s and $\bar{B}$ =21.1 T. However, as in all the HFD obtained for different irradiated samples, the same well defined hyperfine field values were present, the spectra could also be fitted with discrete components having rather broad lines.

To check if the melted layer is amorphized or not, GIXD measurements were performed on various samples. In figure 7 are shown the X-ray diffraction patterns obtained with an untreated sample and with a sample irradiated with 4 shots at a rather low (0.5 J/cm^2) fluence. The two main peaks are due to martensite and the small peaks are attributed to carbide precipitates. Irradiation using a low energy density produces two effects in the X-ray pattern (fig. 7b) : a shift of the line located at $2\theta = 65°$ which is attributed to the presence of tensile residual stresses at the surface of the sample and the appearance of two new lines characteristic of austenite. After irradiation with 20 shots at 3 J/cm^2 the GIXD pattern (fig. 8) displays the retained austenite as well as the presence of new peaks attributed to Fe_5C_2-like carbide precipitates. These peaks are not sharp but, anyway, it is clear that the surface is not amorphized.

Then the hyperfine field distributions as shown in figure 6c were assumed to be the result of an overlapping of various well defined components due to different carbides. In the literature, θ-Fe_3C is characterized by a magnetic component with B= 20.8 T [23,26], χ-Fe_5C_2 by three hyperfine fields (11.0 T, 18.5 T and

22.0 T) [27,28] and ϵ-Fe_2C by also three magnetic components (13.0 T, 17.3 T and 23 T) [29,30]. All these values were found in the hyperfine field distribution (fig. 9). The hyperfine distributions have been therefore analyzed attributing field interval 18.5-21.5 T to cementite Fe_3C, intervals 13-18 T and 23-28 T to ϵ-carbide, intervals 9-12.5 T, 18-19 T and 21.5-23 T to Hägg carbide Fe_5C_2. However, least-square fits assuming Lorentzian lines confirm a predominant presence of ϵ-Fe_2C and cementite. Yet the relative intensity of the component with B $\simeq$ 24 T is too large compared to the intensity of the component with B $\simeq$ 17 T to be attributed to ϵ-Fe_2C only. Some carbides ϵ-$Fe_{2+x}C$ with $x \simeq 0.4$ could be produced in addition [24].

To determine the depth distribution of the carbides, successive electrochemical polishings of the surface were performed. Figure 10 shows CEMS spectra obtained for an as-irradiated sample and after cumulated etchings of 0.3, 0.6 and 1.0 μm. The abundance of carbides decreases rapidly from 41% for the as-treated sample to less than 3% after the removal of 1.0 μm of material. This evolution shows that carbides are only located in the melted layer which thickness is confirmed to be 1 μm. It is worthwhile to note that austenite abundance does not change in this surface layer. Even after etching of 3 μm austenite decreases slightly (fig. 11b). A CXMS measurement (fig. 11c) showed that austenite is distributed in a rather thick heat affected zone. Further CEMS measurements were performed using the same sample after etchings of 3, 6, 9, 12, 15, 18 μm. It is shown (table 3) that austenite decreases slowly and that the thickness of the thermally affected zone is about 20 μm.

Nuclear backscattering measurements show that carbon is not uniformly distributed in the treated zone and that a large oxygen surface peak is present (fig. 12). As no Si diffusion toward the surface is evidenced, 2.43 ωt% Si was introduced as a fixed value in the theoretical simulation of the NBS spectra. The obtained depth profiles of C, O and N for a nodular iron treated with 20 shots of 3 J/cm^2 energy

density are shown in fig. 13. By changing the impact point of the incident alpha beam on the surface, it was found that the treated surface is not homogeneous and only mean values of atomic concentration are given. It appears a rather narrow oxygen distribution in the outermost layers with a surface concentration of about 30 at %. Oxygen is mainly distributed in the first 0.1 μm. Deeper, up to 0.7(1) μm, the oxygen atomic concentration remains equal to $\sim$ 1%. Due to a well-known competition between oxygen and carbon atoms [32], the maximum (27(3) at %) of C distribution is shifted at $\sim 0.08\,\mu$m. Carbon distribution exhibits a plateau and, beyond 0.7(1) μm it decreases to reach the bulk value around 1 μm in depth. Nitrogen atoms from air are also introduced by the laser processing. They are distributed near the surface with a maximum concentration of 9 at %. A small nitrogen amount ($\sim$ 0.5 at %) is present up to 0.6 μm.

This analysis was performed on different samples. A good correlation between the amount of oxygen and the intensity of the paramagnetic component in the CEMS spectra was found. This correlation could allow to attribute this paramagnetic component to the formation of an oxide.

Discussion

From 0.5 J/cm^2 to 3 J/cm^2 the abundance of austenite increases with the fluence for a limited number of 8 pulses but, for higher fluences and/or high number of pulses, the melted layer contains new carbides thus decreasing the relative amount of austenite detected by CEMS (fig. 5). The austenite forms at the expense of martensite. Both phases precipitate with fine grains as evidenced by SEM observations (fig. 1b), which confirms that martensite detected by CEMS is new martensite. The fineness of the microstructure is due to high cooling rate. A rough estimation of temperature profile during cooling was made using the calculation code "ZEBULON" of the

"Ecole des Mines de Paris" based on the solution given by Carslaw and Jaeger [33]. The 1D-calculation concerned the cooling of a melted layer (0.5 or 2 μm in depth) of iron initially at 1500° C or a room temperature homogeneous substrate of thermophysical characteristics of nodular iron. The results are in keeping with earlier simulations [34,35] and give cooling rates in the range 5×10^6 - 10^8 K.s^{-1} depending on the thickness of the melted layer. As the melt depth increases the cooling rate decreases with the energy density. This evolution could be compared with results obtained with laser treated steels [36] showing an increase of austenite amount as the cooling rate decreases, for cooling rates in the range 10^3 - 10^5 K.s^{-1}. However, the austenite amount depends on the number of laser pulses (fig. 5). At a repetition rate of 30 Hz, the melt depth does not depend on the number of pulses suggesting that the cooling rate is not the main parameter for setting up the final microstructure in the melted layer. In contrast, the high amount of C detected by NBS can explain the presence of austenite due to stabilization effect of this element. Carbon is ablated from the graphite nodules during the laser exposure and participates in the formation of a high pressure vapour. Carbon atoms are deposited on the surface and diffuse in the melted matrix. The amount of ablated graphite and the amount of carbon in the melted layer increase with both the fluence and the number of pulses as a cumulative effect. According to the evolution of the atomic fraction of austenite, a characteristic parameter of the treatment concerning phases fractions seems to be the total laser fluence cumulated after successive laser pulses. The average depth of graphite ablation is about 5 μm after 20 pulses of fluence of 3 J/cm^2.

In the repulsion model of carbon in austenite, the probability of having no carbon first nearest neighbour for a Fe atom is 1-6 x, where x is the proportion of occupied octahedral sites in the fcc lattice, i.e. the carbon atomic content in austenite [25,31]. Thus, the relative intensity RI of the $\Gamma_{1,0}$ component in the total

amount of austenite is related to the C content in austenite : RI($\Gamma_{1,0}$)=6x. It was found that C content increases from 5.5 at % to 10.3 at % when the fluence ranges from 0.5 J/cm^2 to 5 J/cm^2 for 8 laser shots. It is worthwhile to note that the maximum C content usually allowed in austenite is about 10 at % when the Fe_8C ordered structure with some vacancies in the carbon sublattice is obtained [18]. This result indicates a large efficiency for graphite ablation when the fluence is high. As well, at a fixed energy density, the C content in austenite increases as a function of the number of shots. The average carbon content x in the outermost surface of the melted zone probed by CEMS can be calculated from the carbon content in austenite given by the repulsion model and from the estimation of carbon contents in both martensite and carbides :

$$x = \frac{n}{100 + n(Si) + n} \times 100$$

with

$$n = RI(A) \times \frac{x_A}{100 - x_A} + RI(M)\frac{x_M}{100 - n(Si) - x_M} + RI(C)\frac{x_C}{100 - x_C}$$

where n and n(Si) are the number of carbon and silicon atoms for 100 iron atoms respectively. The assumption can be made that silicon is only within martensite. RI(A), RI(M), RI(C) are the relative intensity of austensite, martensite and carbides in the CEM spectra respectively, independently of the relative intensity of oxides. x_A, x_M, x_C are the atomic content of C in austenite, martensite and carbides respectively.

The calculation gives an average carbon content in agreement with NBS results. The estimation shows a continuous increasing of average carbon content with the total fluence. Results versus the energy density after 8 pulses are reported in fig. 14. After 8 pulses of 5 J/cm^2 the amount of C (13%) is higher than the maximum carbon solubility in austenite. In these conditions the following transformations occur during cooling from liquid (L) :

$$
\begin{aligned}
L &\longrightarrow L+\gamma \\
L+\gamma &\longrightarrow \gamma\ (\text{saturated})\ +\ \text{carbides} \\
\gamma+\ \text{carbides} &\longrightarrow \gamma+\alpha'+\ \text{carbides}
\end{aligned}
$$

In the same figure is plotted the relative contribution as a function of the depth of the hyperfine field distribution attributed to the formation of different cabides (Fe_2C, Fe_3C, Fe_5C_2). It appears that this contribution is limited to a depth layer of about 1 μm corresponding to the melted zone. NBS showed that C is very abundant in the first 80 nm and that a plateau extends up to 0.7 μm. These results are very well correlated with the abundance of carbides detected by CEMS. Whatever the fluence, ϵ-Fe_2C is always the most abundant (40 %) among the three carbides. The amount of carbides increases with the total deposited energy and the number of shots.

CEMS measurements performed at different depths and a CXMS measurement show that austenite is distributed in a rather thick layer corresponding to melted and heat affected zones. The profile of the austenite amount is constant in the melted layer according to NBS results which give a steady carbon content in this zone. Due to heat diffusion from the hot melted layer into deeper regions, the subsurface reaches austenite transformation during heating. From the above calculations, a layer of a few micrometers thick is expected to reach 10^3 ^{0}C.

Figure 12 shows that carbon content drops down to its initial value at depth of about 1 μm which corresponds to the bottom of the melted zone. Carbon atoms deposited on the surface only diffuse in the liquid matter since the thermal interaction time is very short. To illustrate this, a characteristic length of carbon diffusion $\sqrt{\mathrm{Dt}}$ in the heat affected zone can be estimated : the diffusion coefficient of carbon in austenite at 10^3 ^{0}C is D= 4.9×10^{-7} cm^2.s^{-1} and the duration t of high temperature stage is less than 10^{-6} s. So $\sqrt{\mathrm{Dt}} < 7 \times 10^{-2}$ μm, confirming that no diffusion occurs in the heat affected layer. During heating, austenite forms by reverse martensitic

transformation (of martensitic nature).

Carbon content in austenite also evolves as a function of the depth. Fig. 15 gives the relative contributions of the phases detected at different depths in the case of a nodular iron sample illuminated with 20 pulses at 4 J/cm^2. The C content in austenite is also indicated. Near the surface austenite is saturated (10.5 at % C) but for layers probed deeper and deeper the carbon content decreases regularly to reach a limit value of 2.2(2) at %. Inside the heat affected zone, austenite is poorer in carbon than at the surface. A higher amount of high temperature austenite transforms into martensite during the cooling as for a lower carbon content the austenite is less stable and the Ms point is higher.

It is to note that the quadrupole splitting of the doublet $\Gamma_{1,0}$ remains constant ($\Delta = 0.75(3)$ mm/s) into the whole affected zone. Its lowest value (0.63 mm/s) at the surface could be due to the presence of some nitrogen contribution as explained by Schaaf *et al.* [20]. Effectively, it is in the first 200 nm that nitrogen is mainly concentrated.

The interpretation of the doublet with QS$\sim$0.9 mm/s is not univocal because, if its intensity at the treated surfaces is correlated with the number of oxygen atoms measured by NBS, its evolution as a function of the depth (fig. 15) does not follow the oxygen depth profile. In fact this doublet could be due to two contributions : a thin layer of Fe_2O_3 or Fe_3O_4 oxide and fine dispersed carbides. However oxides are found in successive CEMS measurements as a function of the depth because they are formed during each electrochemical etching. The formation of wüstite $Fe_{1-x}O$ is excluded as the isomer shift of the doublet lies always in the range 0.3-0.4 mm/s, which is not in keeping with previous results by Schaaf *et al.* [21].

Conclusion

Excimer laser processing of martensitic nodular iron leads to a melted layer of about 1 μm above a heat affected zone of about 10 μm in depth. The phases formed are austenite, martensite and carbides. The austenite fraction in the melted layer increases with laser energy density and number of pulses mainly due to the increase of carbon in this zone. When the molten layer contains more carbon than the maximum solubility in austenite, carbides are formed during cooling. Carbon content in austenite also increases with the accumulated energy density. Microstructural changes occur in the heat affected layer without any diffusion by reverse transformation of martensite and lead to partial austenization after cooling.

Acknowledgement :

This work could not have been accomplished without the dedicated effort of Drs O. Uteza and M. Sentis of "Institut de Mécanique des Fluides de Marseille", M. H. Burlet of "Ecole des Mines de Paris" for thermal calculation and L. Vidal of "Institut de Physique Nucléaire de Lyon". Many thanks to all of them.

References

[1] W. Reitz and J. Rewers, Proc. "S.M.T. VI", 1992, Chicago, USA, eds T.S. Sudarshan and J. Braza (T.M.S., Warrendale, USA, 1993) p. 521.

[2] R.K. Singh and J. Viatella, J. Mat., 3(1992)20.

[3] J.E. Montagne, T. Sarnet, C. Prat, G. Inglesakis and M. Autric, Appl. Surf. Sci., 69(1993)108.

[4] A.J. Pedraza, J. Met., 39, 2(1987)14.

[5] S. Tosto, P. Di Lazzaro, T. Letardi and S. Martelli, Proc. "Excimer Lasers and Applications", 1988, Hamburg, Germany, ed. D. Basting (S.P.I.E., Bellingham, USA, 1023(1988)p. 208.

[6] M. Sorescu and E.T. Knobbe, J. Mater. Res., 8(1993)12.

[7] A.S. Brandsen, J.H.P.C. Megaw, P.H. Balkwill and C. Westcott, J. Mod. Opt., 37(1990)813.

[8] A. Emmel, E. Schubert, G. Meyer and H.W. Bergmann, Proc. of EUREKA 205 Int. Workshop "Excimer Laser Applications" 1993, Erlangen, Germany, eds. H.W. Bergmann and K. Schutte (Erlangen, 1993) p. 96.

[9] C. Papaphilippou, A. Fontes, B. Dubrujeaud, M. Vardavoulias and M. Jeandin, Proc. 6 th Int. Congress on Tribology (EUROTRIB), Budapest 1993, ed. M. Kozma (Hungarian Chemical Soc., Budapest) 3(1993)26.

[10] E. Schubert, R. Queitsch, H.W. Bergmann and K. Schutte, Proc. of EUREKA 205 Int. Workshop "Excimer Laser Applications" 1993, (Erlangen, 1993) p. 11.

[11] A. Fontes, M. Jeandin, O. Uteza, M. Sentis and M. Frainais, Mat. and Manuf. Proc., 9(1994)415.

[12] D. Pantelis, A. Tissandier, A. Manousaki and E. Hontzopoulos, Surf. Coating Tech., in press (1994).

[13] E.V. Yakshtas, Yu.Y. Reksnis, R.V. Kanapenas, A.P. Amulyavichyus, R.Yu. Davidonis and K.V. Mararyunas, Phys. Met. Metall., 66(1988)185.

[14] M. Carbucicchio, G. Sambogna and G. Palombarini, Hyp. Inter., 28(1986)1021.

[15] L. Blaes, Ph. Bauer, U. Gonser and R. Kern, Z. Metallkde, 79(1988)278.

[16] P. Schaaf, Ph. Bauer and U. Gonser, Z. Metallkde, 80(1989)77.

[17] P. Schaaf, Ph. Bauer and U. Gonser, Hyp. Inter., 46(1989)541.

[18] P. Schaaf, V. Biehl, U. Gonser, M. Bamberger and Ph. Bauer, J. Mater. Sci., 26(1991)5019.

[19] G. Rixecker, P. Schaaf and U. Gonser, J. Phys. D : Appl. Phys., 26(1993)870.

[20] P. Schaaf, A. Emmel, E. Schubert, H.W. Bergmann and K.P. Lieb, in Proc. Int. Conf. "ICAME'93", Vancouver, Hyp. Int. (to be published).

[21] G. Le Caër and J.M. Dubois, J. Phys. E : Sci. Instrum., 12(1979)1083.

[22] J. Foct, J.M. Dubois and G. Le Caër, J. de Phys., 35, C6(1974)493.

[23] H. Ino, T. Moriya, F.E. Fujita, Y. Maeda, Y. Ono and Y. Inokuti, J. Phys. Soc., Japan, 25(1968)88.

[24] O.N.C. Uwakweh, Ph. Bauer and J.M.R. Genin, Metall Trans. A, 21A(1990)589.

[25] Ph. Bauer, O.N.C. Uwakweh and J.M.R. Genin, Hyp. Inter., 41(1988)555.

[26] T. Shinjo, F. Itoh, H. Takaki, Y. Nakayama and N. Shikazono, J. Phys. Soc. Japan, 19(1964)1252.

[27] H. Bernas, I.A. Campbell and R. Fruchart, J. Phys. Chem. Sol., 28(1967)17.

[28] C.B. Ma, T.Ando, D.L. Williamson and G. Krauss, Metal. Trans., 14A(1983)1033.

[29] G. Le Gaër, J.M. Dubois, M. Pijolat, V. Perrichon and P. Bussière, J. Phys. Chem., 86(1982)4799.

[30] R.A. Arents, Yu.V. Maksimov, I.P. Suzdalev, V.K. Imshennik and Yu.F. Krupyanskiy, Fiz. Mat. Metalloved, 36(1973)277.

[31] H.J. Aaronson, H.A. Domian and G.M. Pound, Trans. TMS-AIME, 236(1966)753.

[32] M.A. El Khakani, H. Jaffrezic, G. Marest, N. Moncoffre and J. Tousset, Nucl. Instr. Meth. in Phys. Res., B50(1990)406.

[33] H.S. Carlaw and J.C. Jaeger in "Conduction of Heat in Solids", Oxford University Press, London, 2^d ed, (1959) p. 62.

[34] G. Antony and P.R. Strutt, Proc. "Science and Technology of Rapidly Quenched Alloys", Boston, 1986, Ed. Tenhover *et al.*, Mat. Res. Soc. Symp. Proc. Vol. 80 (1987) p. 231.

[35] C. Maier, P. Schaaf and U. Gonser, Mater. Sci. and Eng., A150(1992)271.

[36] V.S. Kraposhin, K.V. Shakhlevich, T.M. Vyaz'mina, Metallovedenie i Termicheskaya Obrabotka 10(1989)21, Engl. Trans. Metal Science and Heat Treatment, Sept-Oct. (1989).

Table 1

Global weight composition of nodular iron and atomic composition of the matrix.

	C	Si	Mn	Cr	Ni	Mo	S	Cu	Sn	Mg	P
Nodular Iron (wt%)	3.50	2.43	.70	.05	.03	.02	.007	.05	.005	.061	.00
Matrix (at%)	~2.2	5.5	.7	.05	.03		.012		.015		.00

Table 2

Relative contributions of phases detected by CEMS at the surface of a nodular iron irradiated with different number of laser pulses of 2 J/cm^2 fluence.

Pulses	4	8	20	40
Martensite	77	69	58	45
Austenite	6	20	27	57
Doublet	17	11	15	3

Table 3

Relative contributions of the phases detected by CEMS at different depths from the surface in a nodular iron irradiated with 20 pulses of 4 J/cm^2 fluence.

Depth (μm)	Surface	0.3	0.6	1	3	6	9	12
Martensite	30	43	47	52	68	76	77	86
Austenite	22	21	29	21	16	13	13	12
Carbides	39	24	9	4	3	3	3	0
Doublet	9	12	15	23	13	8	7	2

Figure Captions

Fig. 1. a) Polarized light optical micrograph of martensitic nodular iron irradiated by one laser pulse of 3 J/cm^2 fluence.

b) SEM cross-section of the treated zone after "Nital etching" - Martensitic nodular iron irradiated with 40 pulses of fluence 5 J/cm^2 at frequency of 1 Hz.

Fig. 2. CEMS spectra for nodular iron irradiated with 4 and 8 XeCl laser pulses of 1 J/cm^2. The CEMS spectrum corresponding to the untreated sample is shown at the bottom of the figure.

Fig. 3. CEMS spectra for nodular iron irradiated with XeCl laser pulses of 1.5 J/cm^2. The repetition rate is 30 Hz.

Fig. 4. CEMS spectra for nodular iron irradiated with XeCl laser pulses of 3 J/cm^2. The repetition rate is 30 Hz.

Fig. 5. Evolution of austenite fraction versus the laser beam energy density for various number of shots at a frequency of 10 Hz.

Fig. 6. a) CEMS spectrum of nodular iron treated with 20 shots of 3 J/cm^2. b) Spectrum obtained after substraction of the "crystalline part. c) Corresponding hyperfine field distribution.

Fig. 7. Grazing X-ray diffraction pattern ($\alpha = 0.3°$) for an untreated nodular iron (a) and after illumination with one pulse of 0.5 J/cm^2 (b). The arrows show the position of the austenite peaks.

Fig. 8. Grazing X-ray diffraction pattern ($\alpha = 3°$) for a nodular iron illuminated with 20 excimer laser pulses of 3 J/cm^2.

Fig. 9. Hyperfine field distribution corresponding to a nodular iron treated with 20 laser pulses of 4 J/cm^2. The intervals corresponding to Fe_2C, Fe_3C and Fe_5C_2 phases are indicated by ϵ, θ and χ respectively.

Fig. 10. CEMS spectra of laser-treated nodular iron with 20 pulses of 4 J/cm^2 registered at different depths : a) laser-treated surface, b) 0.3 μm, c) 0.6 μm, d) 1.0 μm.

Fig. 11. Mössbauer spectra of laser-treated nodular iron with 20 pulses of 4 J/cm^2 registered by detection of conversion electrons a) at the surface, b) after removal of 3 μm, c) by detection of conversion X-rays.

Fig. 12. NBS spectrum of a nodular iron irradiated with 20 laser pulses of 3 J/cm^2 taken with alpha particles of 7.5 MeV energy.

Fig. 13. Depth profiles of C, N, O elements after laser treatment (20 pulses of 3 J/cm^2) of a nodular iron.

Fig. 14. Carbon content in melted layer of a nodular iron treated with 8 pulses at various energy densities.

Fig. 15. Phase fractions of the sample irradiated with 20 laser pulses of 4 J/cm^2 as a function of the depth. o, □ , △, ◇ symbols represent martensite, austenite, oxide and carbides respectively.

Photo Captions

Fig. 1a : Polarized light optical micrograph of martensitic nodular iron irradiated by one laser pulse of fluence of 3 J/cm^{-2}.

Fig. 1b : SEM cross section of the treated zone after "Nital etching". Martensitic nodular iron irradiated with 10 pulses of fluence of 5 J/cm^{-2} at frequency of 1 Hz.

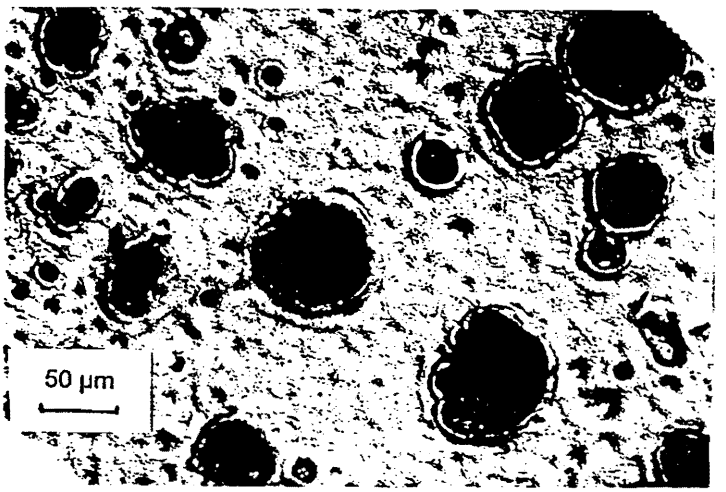

1a

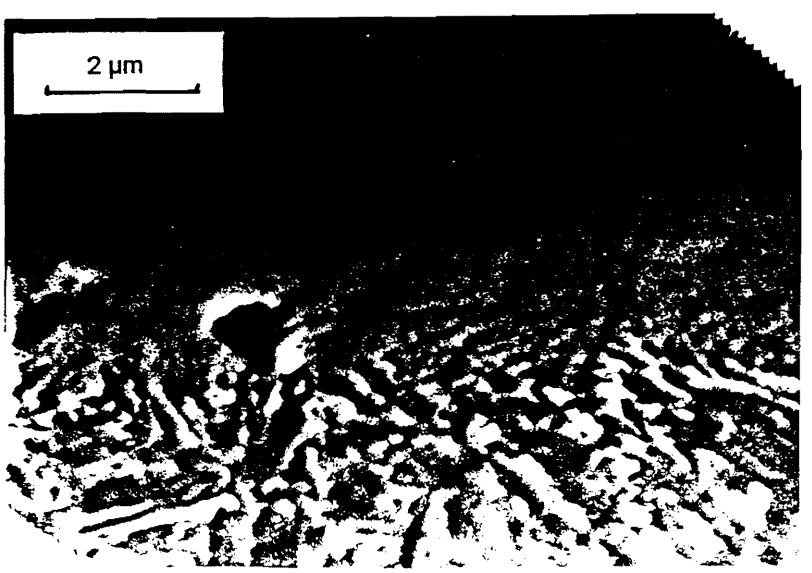

1b

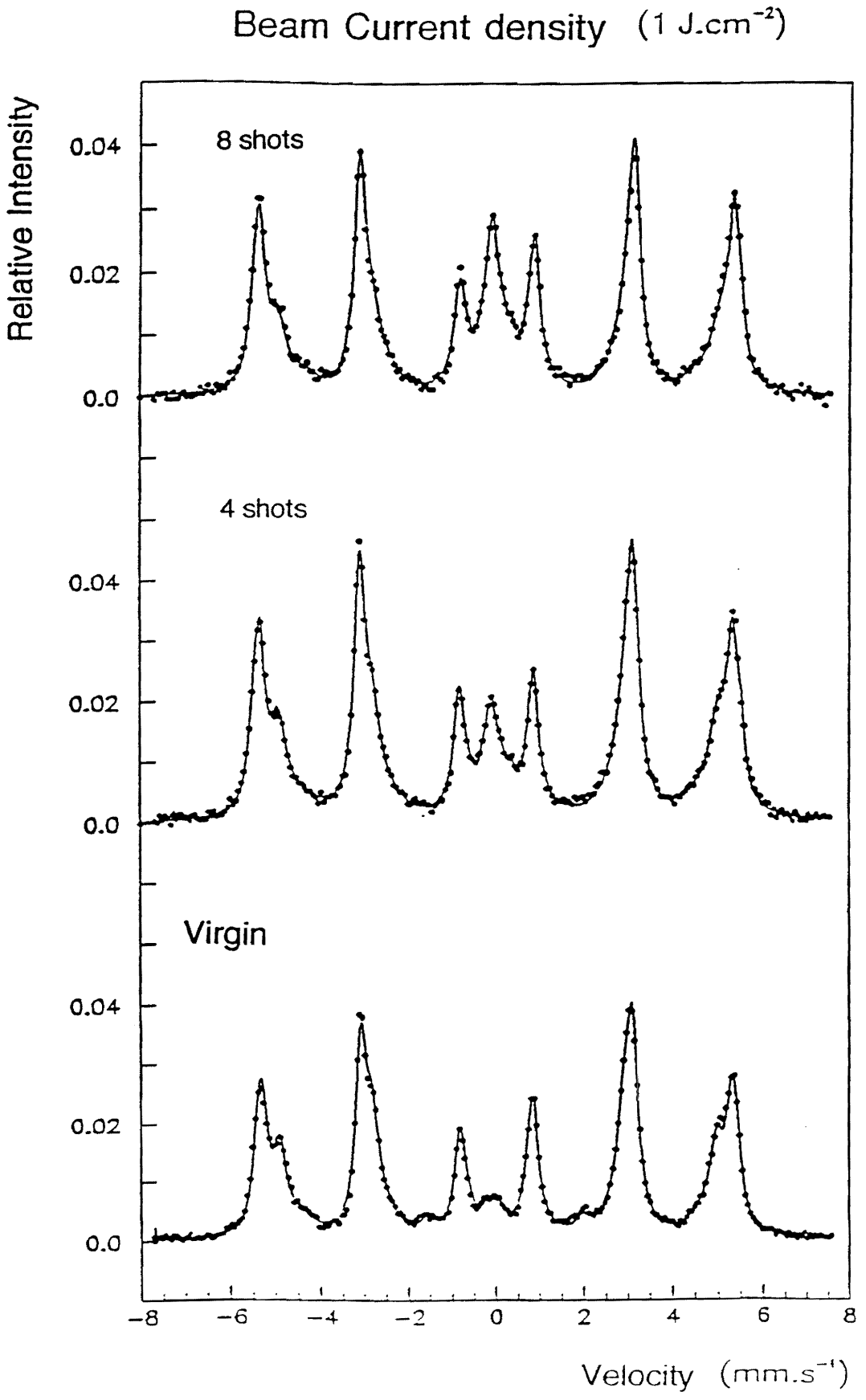
Beam Current density (1 J.cm^{-2})
Relative Intensity
8 shots
4 shots
Virgin
0.04
0.02
0.0
−8
−6
−4
−2
0
2
4
6
8
Velocity (mm.s^{-1})

Fig. 2

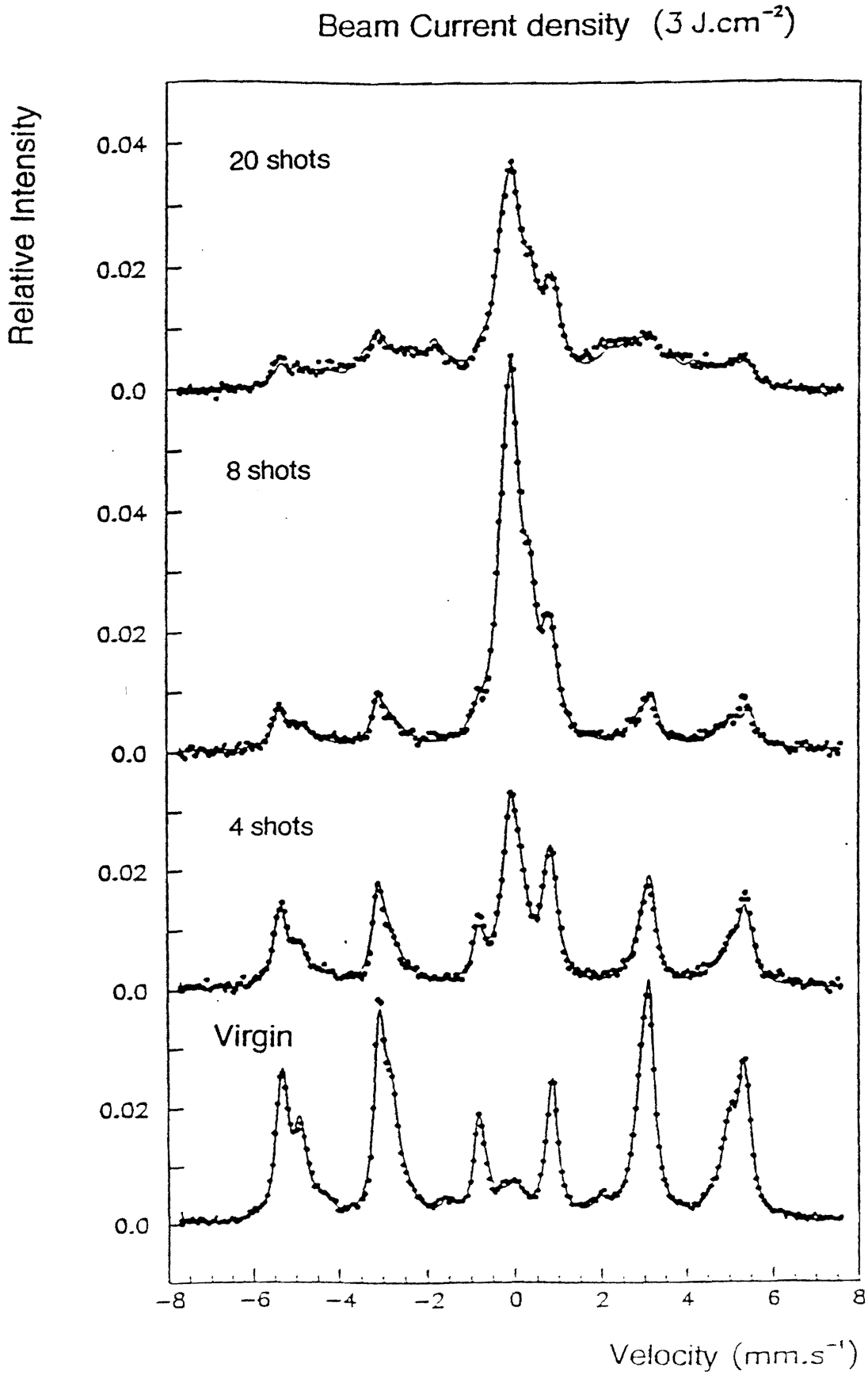
Beam Current density (3 J.cm^{-2})
Relative Intensity
20 shots
8 shots
4 shots
Virgin
0.04
0.02
0.0
−8
−6
−4
−2
0
2
4
6
8
Velocity (mm.s^{-1})

Fig 3

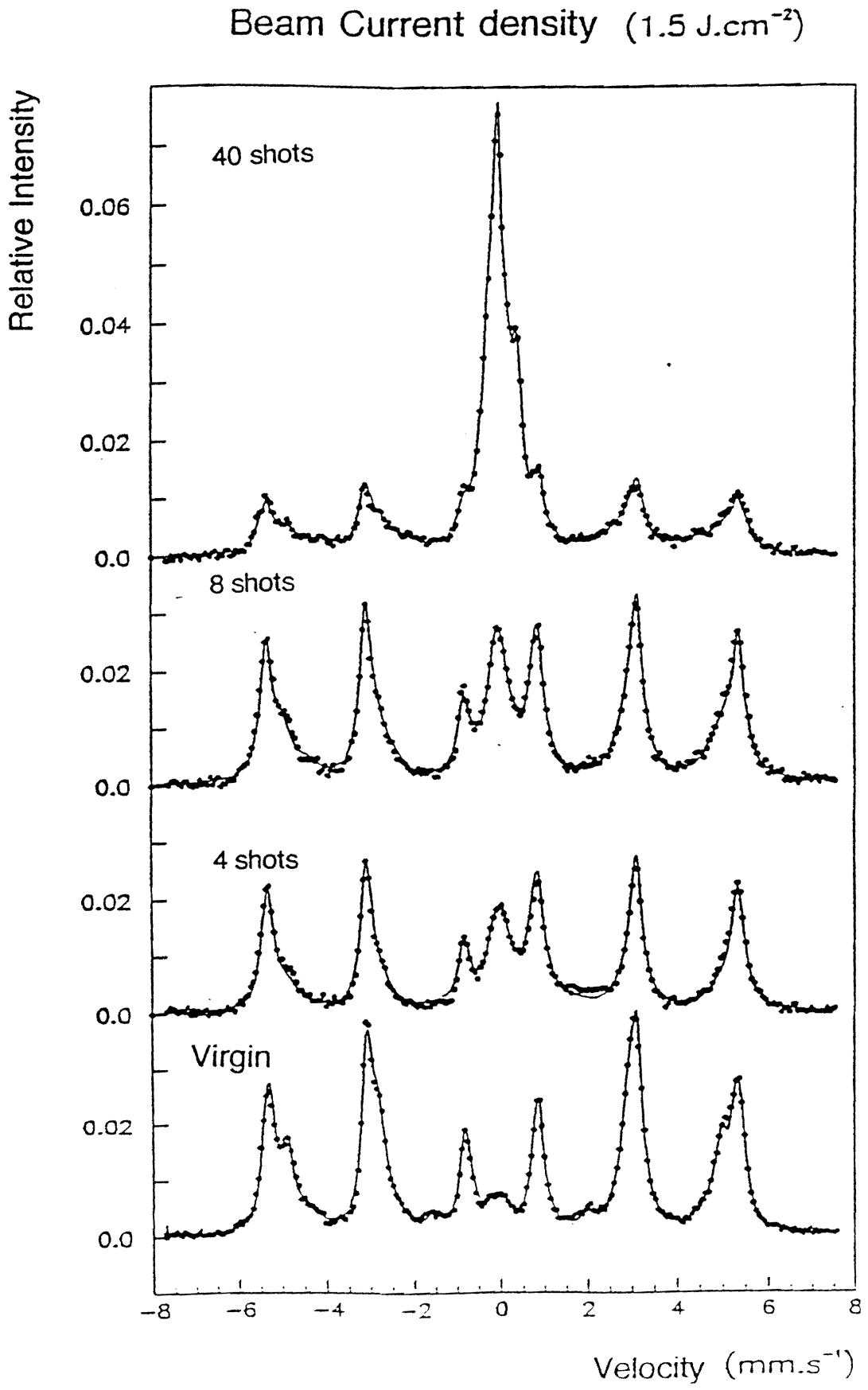
Beam Current density (1.5 J.cm^{-2})
Relative Intensity
40 shots
8 shots
4 shots
Virgin
0.06
0.04
0.02
0.0
−8
−6
−4
−2
0
2
4
6
8
Velocity (mm.s^{-1})

Fig. 6

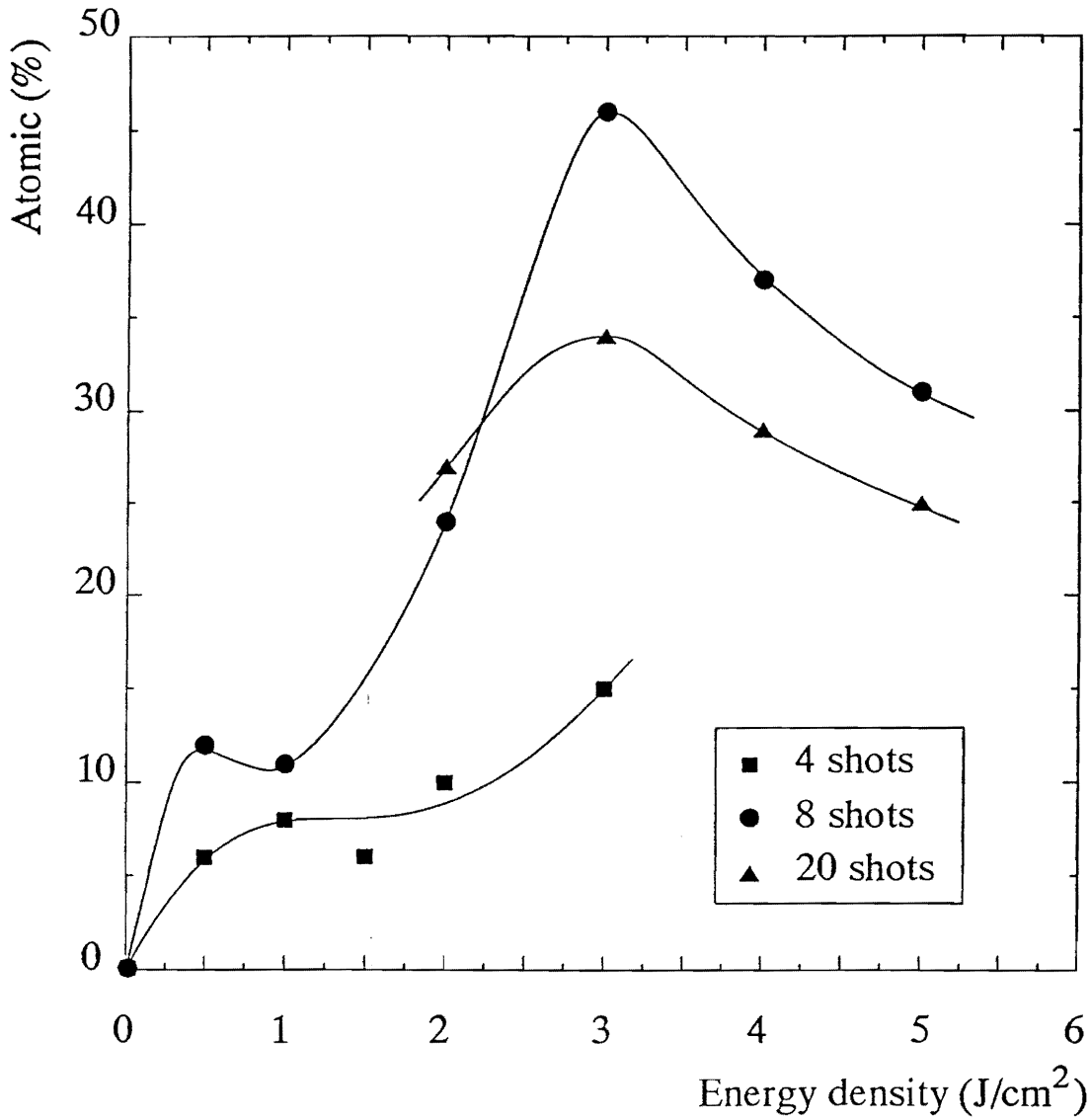
Atomic (%)
50
40
30
20
10
0
0
1
2
3
4
5
6
Energy density (J/cm^2)
4 shots
8 shots
20 shots

Fig 5

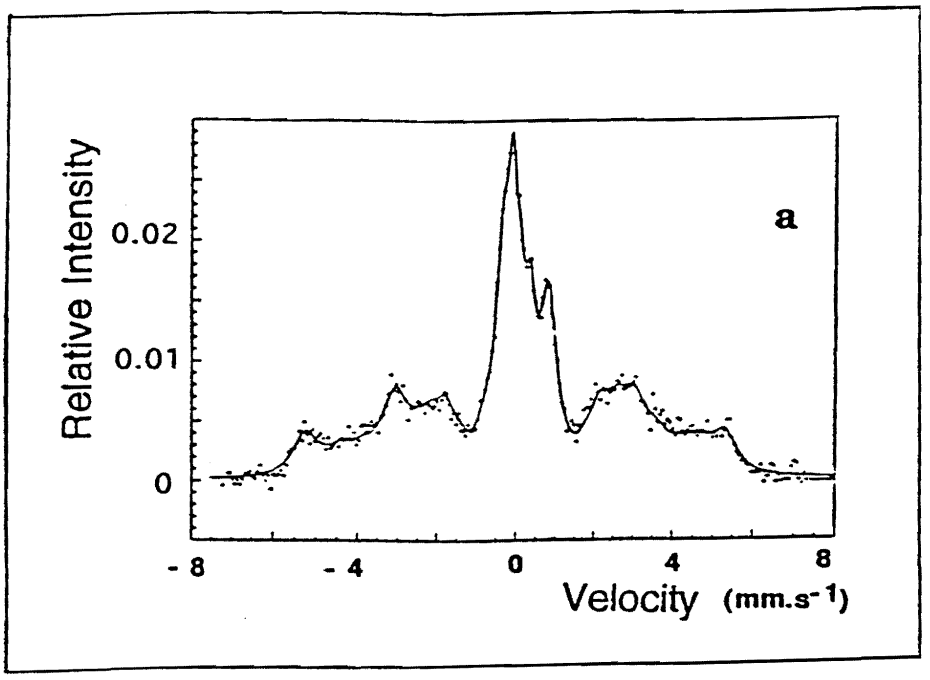
Relative Intensity
0.02
0.01
0
a
- 8
- 4
0
4
8
Velocity (mm.s-1)

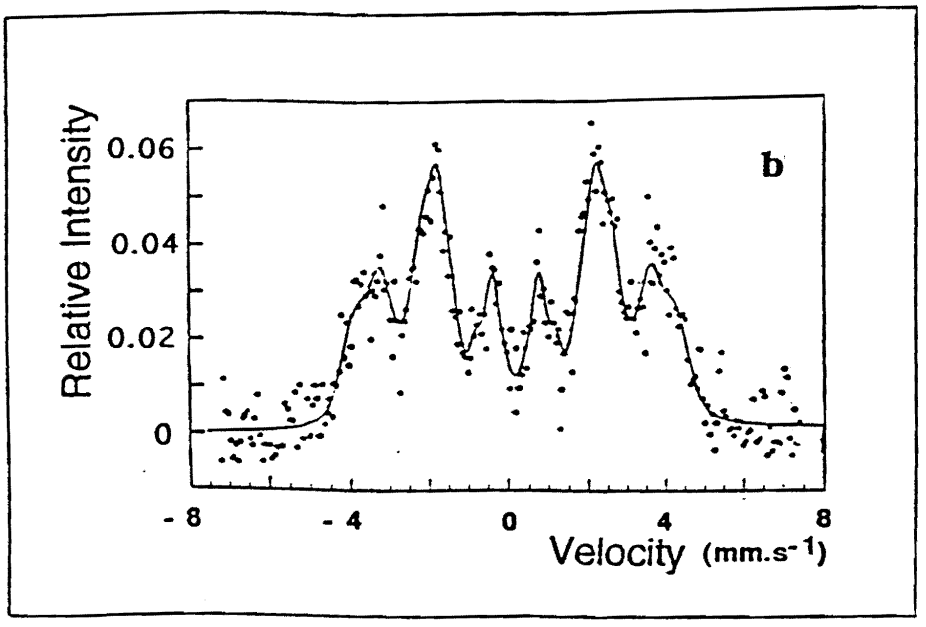
Relative Intensity
0.06
0.04
0.02
0
b
- 8
- 4
0
4
8
Velocity (mm.s-1)

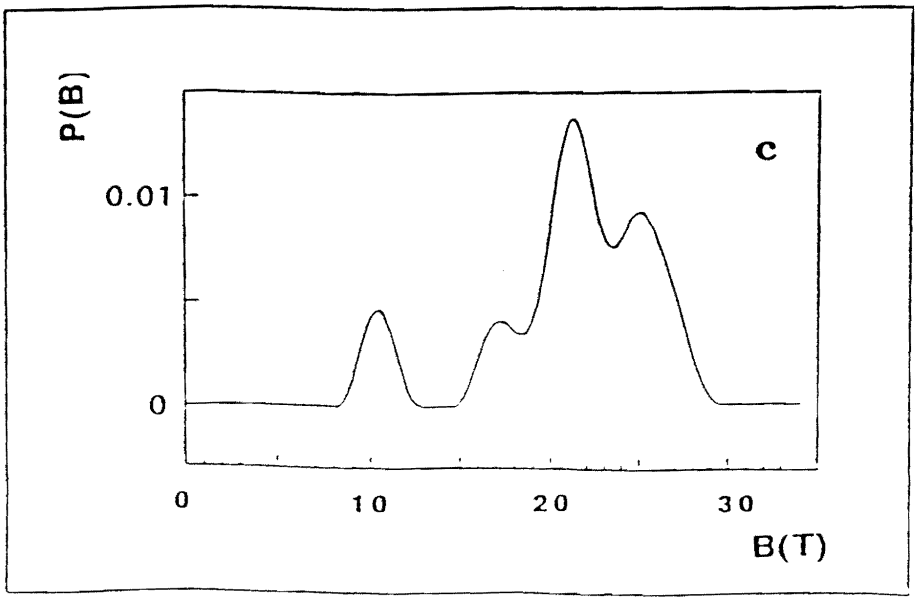
P(B)
0.01
0
c
0
10
20
30
B(T)

Fig 6

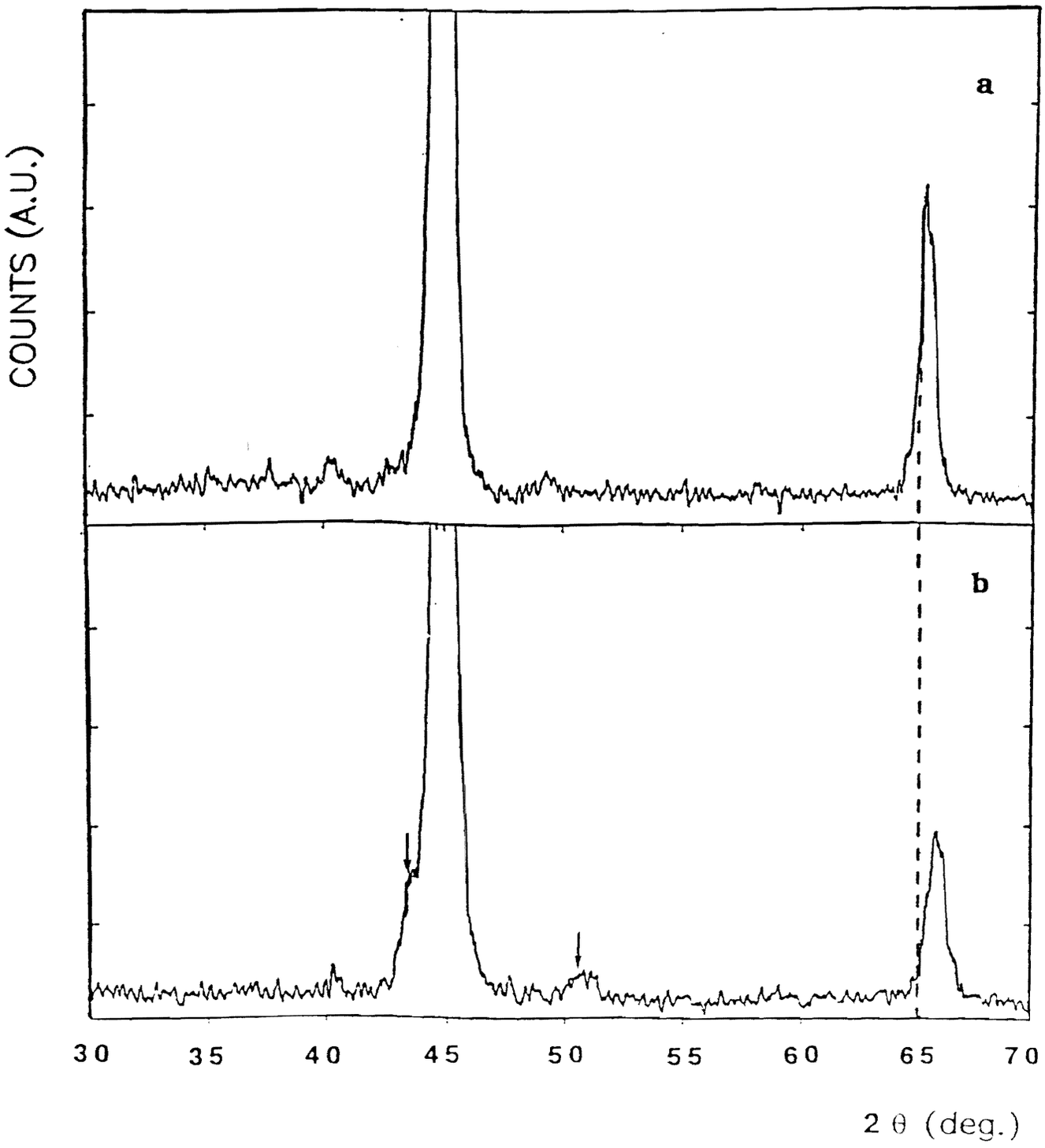

Pu7

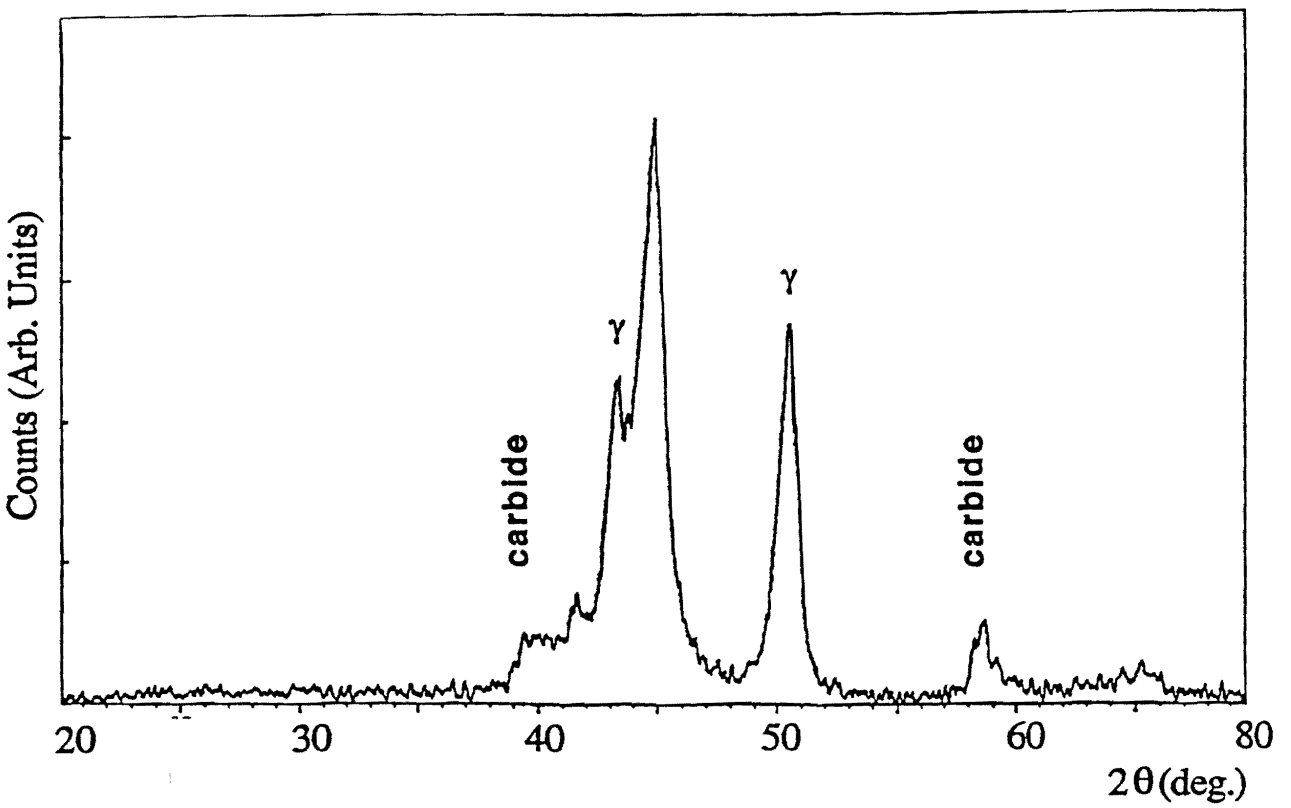

Fig 8

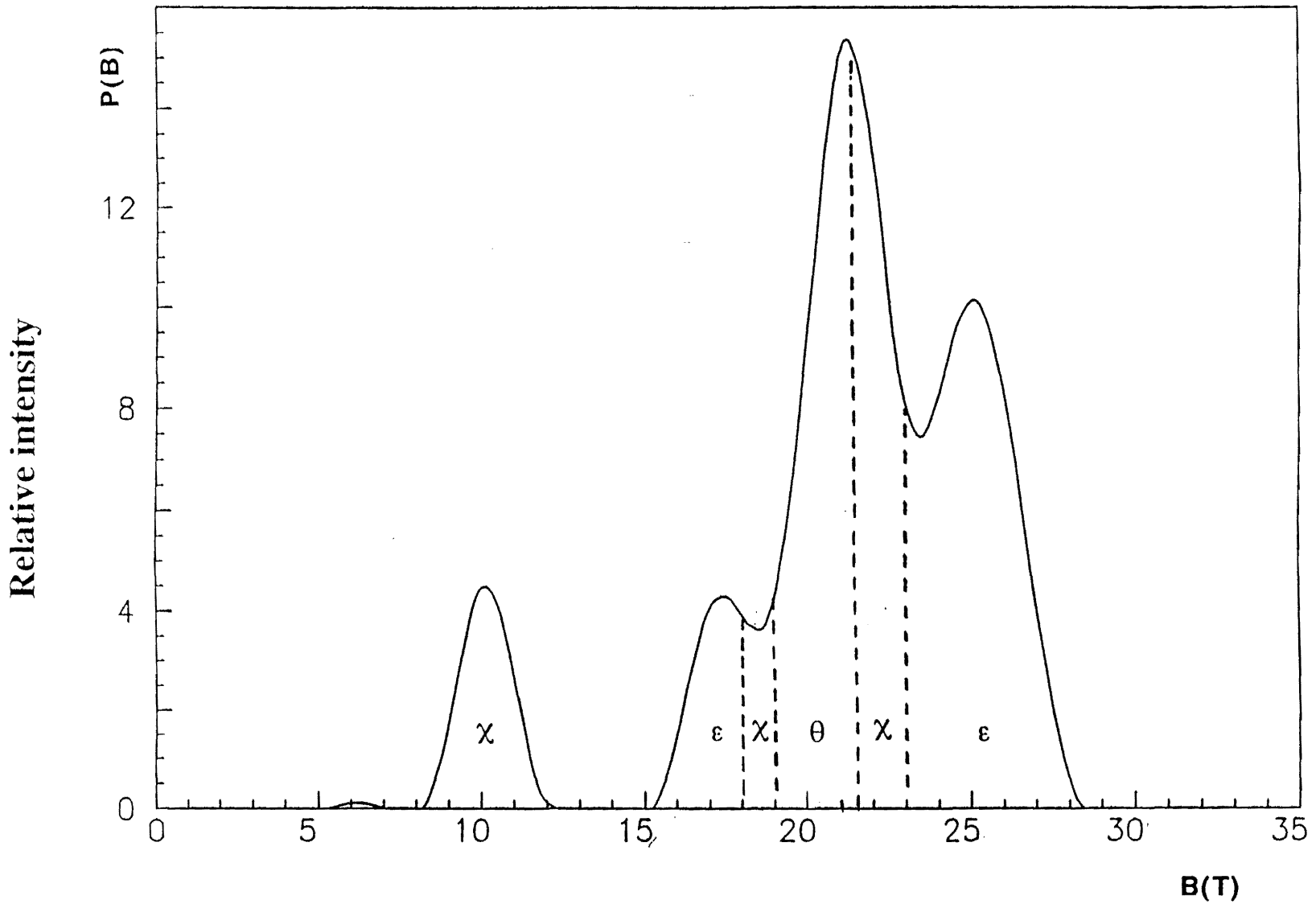
Relative intensity
P(B)
12
8
4
0
0
5
10
15
20
25
30
35
B(T)
χ
ε
χ
θ
χ
ε

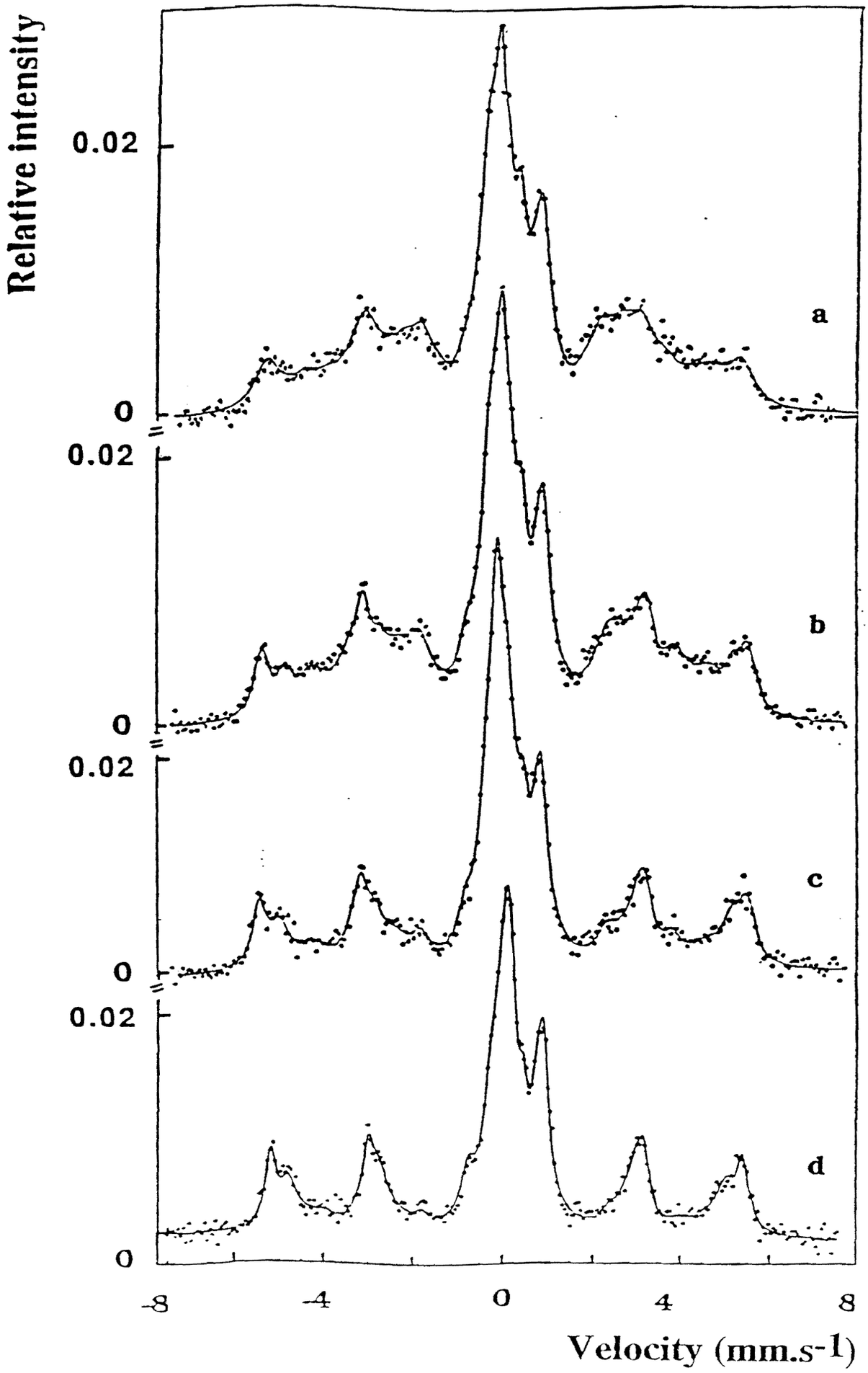
Relative intensity
0.02
0
0.02
0
0.02
0
0.02
0
a
b
c
d
-8
-4
0
4
8
Velocity (mm.s-1)

Fig 10

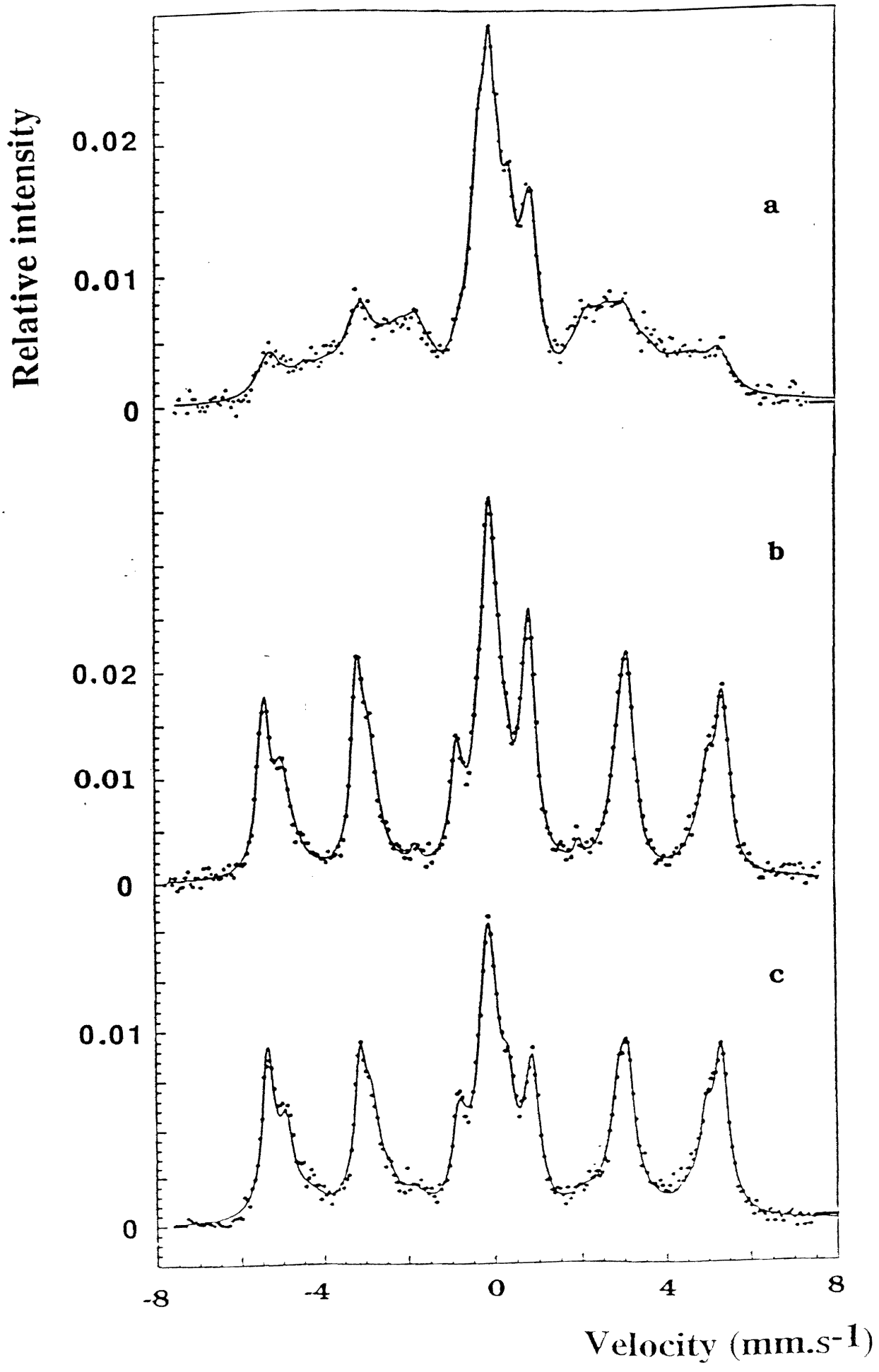

Fig 11

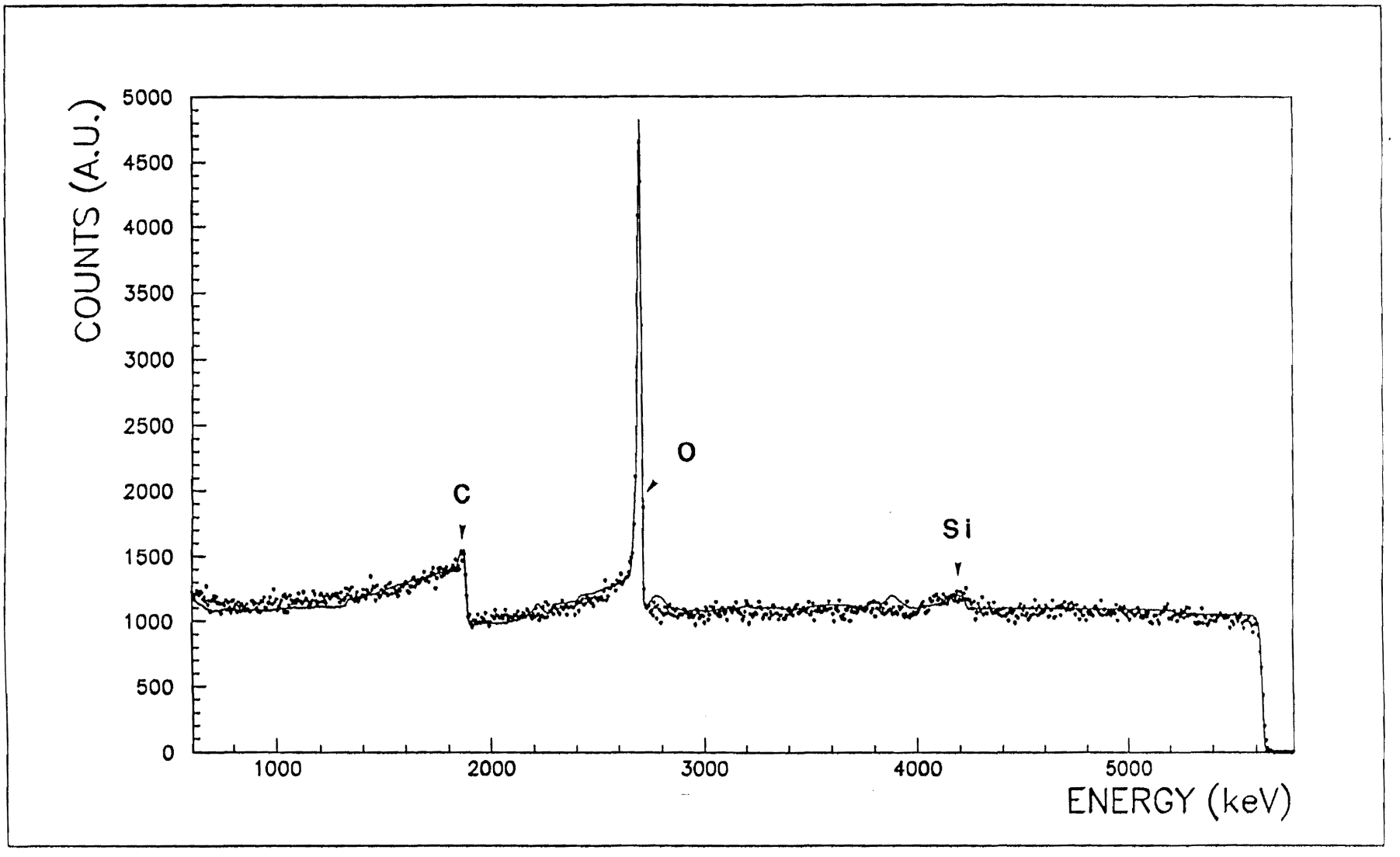
COUNTS (A.U.)
5000
4500
4000
3500
3000
2500
2000
1500
1000
500
0
C
O
Si
1000
2000
3000
4000
5000
ENERGY (keV)

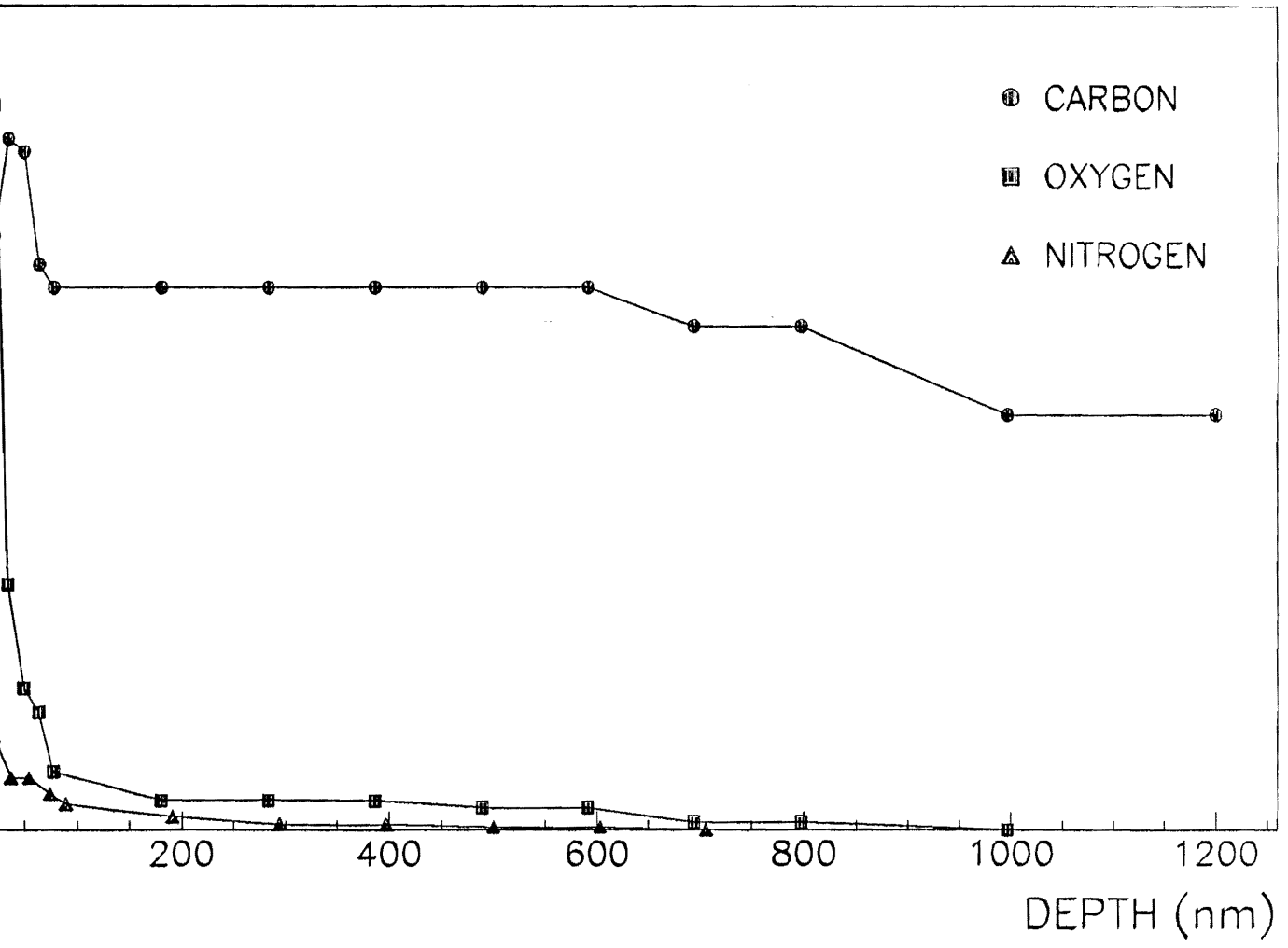
CARBON
OXYGEN
NITROGEN
200
400
600
800
1000
1200
DEPTH (nm)

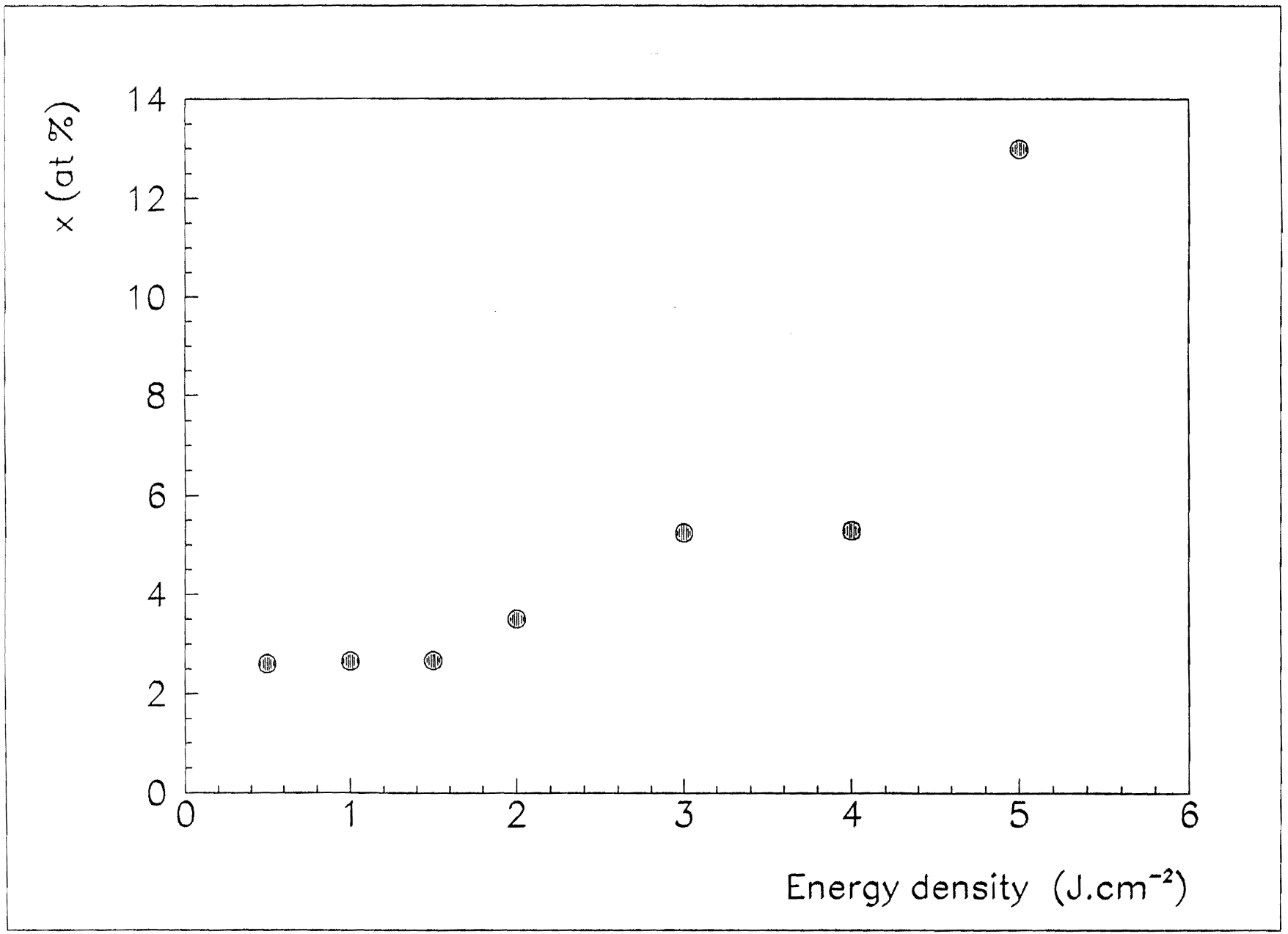

Fig 4

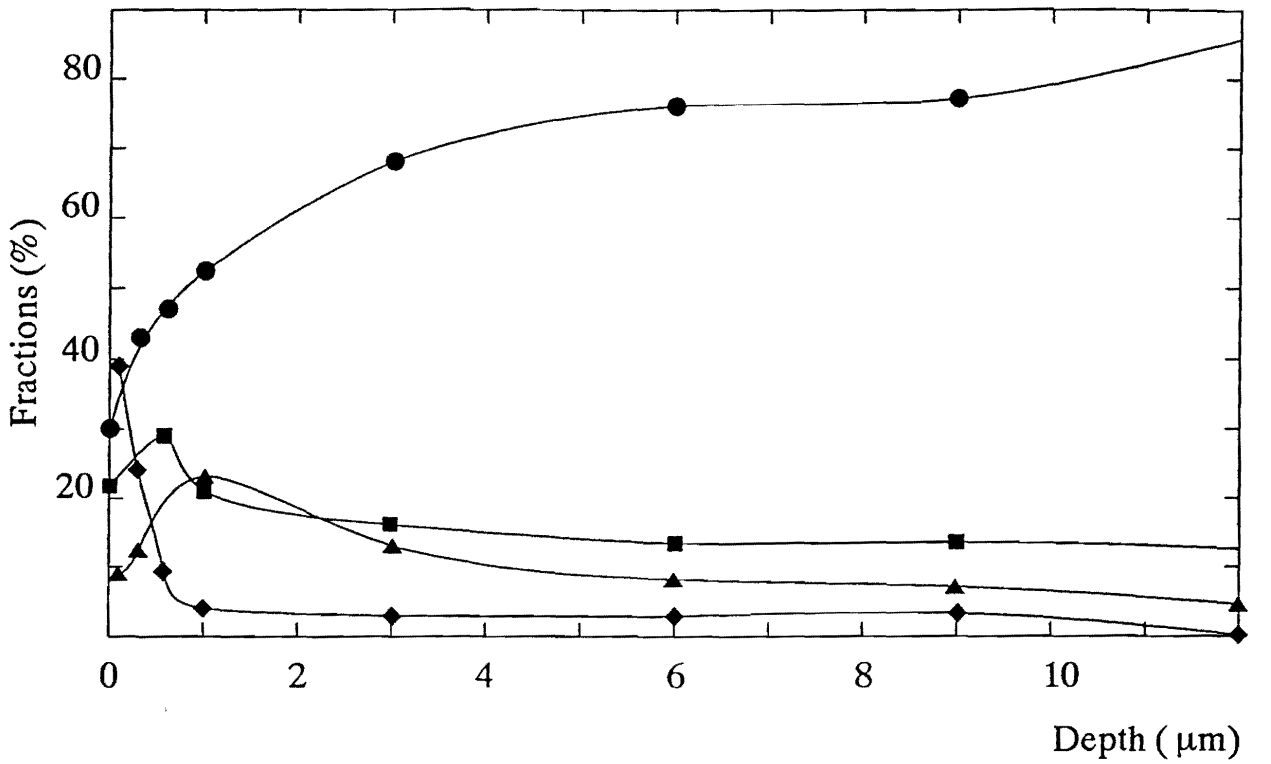
80
60
40
20
Fractions (%)
0
2
4
6
8
10
Depth (μm)